

Optical and magnetic properties of ZnCoO thin films synthesized by electrodeposition

M. Tortosa,¹ M. Mollar,¹ B. Marí,^{1,a)} and F. Lloret²

¹*Departament de Física Aplicada, Universitat Politècnica de València, Camí de Vera s/n, València 46022, Spain*

²*Departament de Química Inorgànica/Institut de Ciència Molecular, Universitat de València, Avda. Dr. Moliner 50, Burjassot 46100, Spain*

(Received 11 December 2007; accepted 5 May 2008; published online 1 August 2008)

Ternary $Zn_{1-x}Co_xO$ crystalline films with different compositions were grown by electrodeposition. The Co content in the final compound is linked to the initial Co/Zn ratio in the starting solution. X-ray diffraction reveals a wurtzite structure for the $Zn_{1-x}Co_xO$ films. Transmittance spectra show two effects proportional to Co content, a redshift of the absorption edge and three absorption bands, which are both interpreted to be due to the Co incorporated into the ZnO lattice. The amount of deposited charge was used to get a precise control of the film thickness. Magnetic measurements point out that Co(II) ions are isolated from each other, and consequently the films are paramagnetic.

© 2008 American Institute of Physics. [DOI: [10.1063/1.2952548](https://doi.org/10.1063/1.2952548)]

I. INTRODUCTION

Diluted magnetic semiconductors (DMSs) have recently received much attention because of complementary properties of semiconductor and ferromagnetic material systems. These materials are promising for spintronic devices because they provide charge and spin degrees of freedom in a single substance. The research on ternary ZnCoO semiconductors has been greatly stimulated by the high Curie temperature for the ferromagnetic transition calculated in bulk materials and found to be around 300 K.¹ As a consequence, ZnCoO could be a good candidate for practical applications in advanced spintronic devices (Ref. 2) if the predicted ferromagnetic behavior is experimentally confirmed.

At present, there are some controversies concerning the magnetic behavior of ternary ZnCoO compounds. Some authors claim they have succeeded in synthesizing materials with intrinsic ferromagnetic behavior.³ Others attribute the origin of the ferromagnetism to different causes such as precipitation of Co_3O_4 (Ref. 4) or extrinsic contamination,⁵ while other authors only report paramagnetic behavior.^{6,7}

This animated interest in obtaining ZnCoO for spintronic applications is promoting big efforts to synthesize thin films by different methods such as molecular beam epitaxy,³ sol-gel,⁴ reactive magnetron cosputtering,^{8–10} and pulsed-laser deposition.^{6,7,11,12} On the other hand, the preparation of zinc oxide by electrodeposition is a well-established technique able to produce good crystalline materials under different morphologies (Refs. 13–15), and recently, two papers related to the synthesis of ternary zinc-related compounds (ZnMgO and ZnCdO) have appeared in the literature confirming that electrodeposition is an alternative method for ternary oxide thin film deposition.^{16,17}

This technique presents some interesting advantages when compared with other methods referred before. Deposi-

tion occurs at low temperature and at atmospheric pressure that is compatible with deposition onto polymer substrates; the film thickness can be directly monitored by the charge consumed during the deposition process. It is a low-cost method that does not require expensive equipment and is environment friendly. Taking advantage of the versatility supplied by electrochemical wet methods, we can foresee that a large variety of oxides will be prepared by electrodeposition in the near future.

In this letter, we report the structural and optical characterizations of ternary $Zn_{1-x}Co_xO$ thin films with different Co contents synthesized by means of the cathodic electrodeposition technique using an organic liquid, dimethyl sulfoxide (DMSO), as electrolyte. The influence of Co content on the structural and optical properties of ternary $Zn_{1-x}Co_xO$ thin films will be discussed. Magnetic susceptibility measurements indicate that our films exhibit a paramagnetic behavior, which corresponds to isolated Co atoms without any magnetic interaction among them.

In an electrochemical procedure, the desired ions present in the bath, previously dissolved from suitable precursors, flow through the electrolyte driven by the action of an applied electric field. Some of them may be deposited on the electrode after undergoing a charge transfer reaction. Concerning the electrodeposition of ZnO, at least three different baths have already been used, namely, aqueous,^{13–15} DMSO,^{17–19} and nitrates.²⁰

II. EXPERIMENTAL DETAILS

The electrodeposition procedure consists of a classical three-electrode electrochemical cell and a solution containing 25 mM of $ZnCl_2$, different concentrations of $CoCl_2$, 0.1M of $KClO_4$ as supporting electrolyte, and dissolved oxygen in a DMSO solution. The bath was maintained at 90 °C without stirring by a thermostat. Glass slides of about 1 × 2 cm coated with fluorine-doped polycrystalline SnO_2 (FTO) with sheet resistances of 10 Ω/sq were used as sub-

^{a)}Author to whom correspondence should be addressed. FAX: +34 963877189. Electronic mail: bmari@fis.upv.es.

strates. Conducting glass substrates, previously cleaned by rinsing with acetone then with distilled water and dried, were set up as working electrodes located near the referential cathode at approximately 1 cm. Potentiostatic deposition was employed by means of a potentiostat/galvanostat to maintain a constant potential during the deposition ($V = -0.9$ V). After deposition, the films were subsequently rinsed with pure DMSO and distilled water.

Films of $Zn_{1-x}Co_xO$ were potentiostatically deposited (-0.9 V) from the dissolution at 90 °C containing both Co^{2+} and Zn^{2+} precursor species. The Co^{2+}/Zn^{2+} atomic ratio in the starting bath was varied by changing the $CoCl_2$ and $ZnCl_2$ concentration ratios between 4% and 30%. The films deposited onto the glass substrates are transparent to the human eye but become blue (commonly known as “blue cobalt”) when the Co/Zn ratio in the starting bath is increased.

Quantitative elemental analysis was obtained by using a JEOL JSM 6300. The structural properties of these films were characterized through x-ray diffraction (XRD). XRD patterns in the Θ - 2Θ configuration were performed using radiation of a copper anticathode ($Cu K\alpha$, 1.54 Å). Optical properties were monitored by transmittance using a Xe lamp in association with a 500 mm Yvon-Jobin HR460 spectrometer using a back-thinned charge-coupled device detector (Hamamatsu) optimized for the ultraviolet-visible spectroscopy range. Magnetic susceptibility measurements (2.0–300 K) were carried out with a Quantum Design SQUID magnetometer. The magnetic susceptibility was measured under an applied magnetic field of 1 T at high temperature ($T > 20$ K) and 100 G at low temperature ($T < 20$ K) to avoid any problem of magnetic saturation. The magnetic data of the sample were corrected for the substrate as well as for the zinc oxide diamagnetism.

III. RESULTS AND DISCUSSION

Figure 1(a) shows a typical energy dispersive x-ray (EDX) spectrum for a $ZnCoO$ sample. The content of different elements in the sample is observed in the spectrum confirming the incorporation of Co into the ZnO matrix. Three lines coming from internal Co transitions located at $0.775(L_\alpha)$, $6.930(K_\alpha)$, and $7.649(K_\beta)$ keV can be identified in the EDX spectrum. Lines corresponding to the other components of the films Zn and O also appear. The Sn lines come from the substrate. The chemical composition of the $Zn_{1-x}Co_xO$ thin films was obtained from the EDX spectra. Quantitative results of the Co/Zn ratio are calculated from the area of the corresponding spectral K lines. The amount of Co in the ternary films has been found to vary between 0.9% and 23% [as shown in Fig. 1(b)] as a function of the initial cations ratio in the starting dissolution.

Figure 2 shows the XRD pattern of four electrodeposited $Zn_{1-x}Co_xO$ films with different Co contents. The diffraction peaks located at 34.42° and 36.25° correspond to the (002) and (101) directions, respectively, of the ZnO hexagonal wurtzite structure. Peaks corresponding to (102) and (103) directions of the wurtzite lattice are still visible for the best crystallized sample $Zn_{0.94}Co_{0.06}O$. The six peaks labeled with stars come from the FTO substrate. The pattern associated

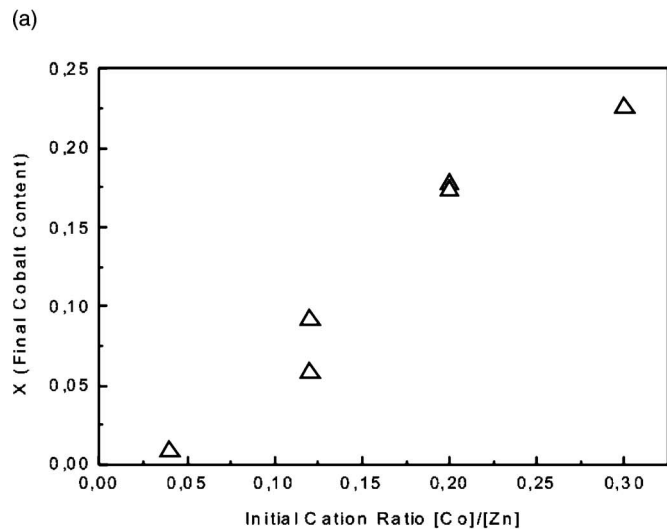
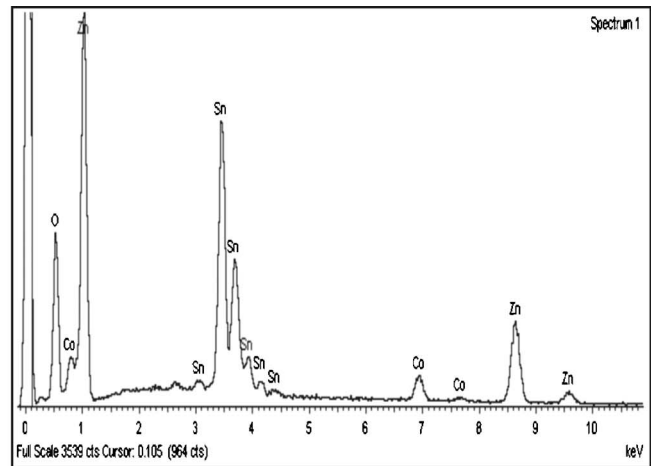


FIG. 1. (a) EDX spectrum of a $ZnCoO$ film obtained from a bath containing a ratio of $[Co]/[Zn]=20\%$. (b) Calculated Cobalt content in the final $Zn_{1-x}Co_xO$ alloy films as a function of the ratio concentrations of cations $[Co]/[Zn]$ in the starting dissolution.

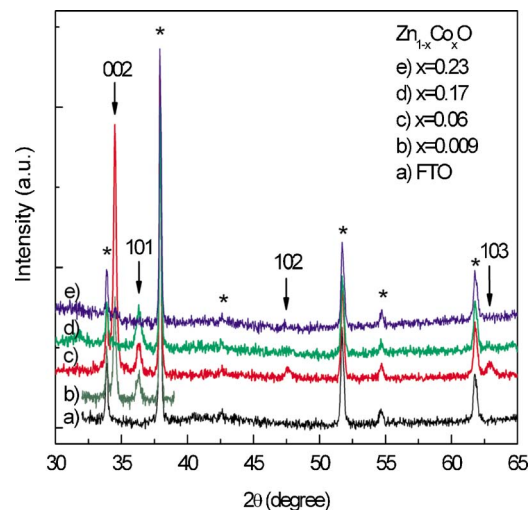


FIG. 2. (Color online) XRD 2θ scan diagram of $ZnCoO$ crystals deposited on FTO covered glass. The spectrum shows the presence of the (002) preferred hexagonal wurtzite orientation. Peaks belonging to different orientations of ITO are identified with (*).

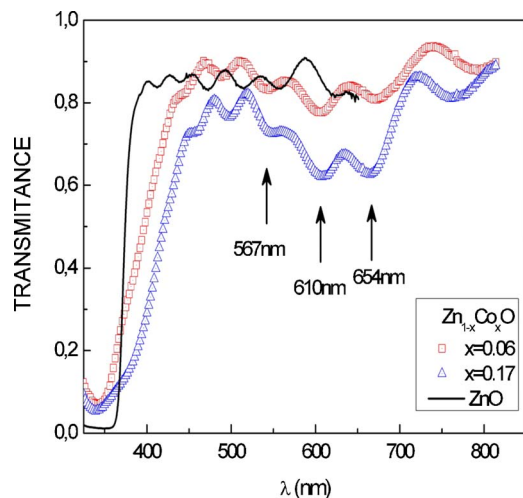


FIG. 3. (Color online) Transmittance of two $\text{Zn}_{1-x}\text{Co}_x\text{O}$ samples compared with a ZnO reference sample.

with the electrodeposited $\text{Zn}_{1-x}\text{Co}_x\text{O}$ layer is identical to that of ZnO with a preferred growth orientation in the (002) direction. Increasing the Co concentration results in pronounced (002) intensity peak reaching a maximum for the $\text{Zn}_{0.94}\text{Co}_{0.06}\text{O}$ sample and practically disappearing for higher Co concentrations. The peak corresponding to the (101) direction reaches a maximum for the $\text{Zn}_{0.83}\text{Co}_{0.17}\text{O}$ film and tends to disappear for higher Co concentrations. This suggests that the ZnO lattice becomes deformed owing to the presence of increasing amounts of Co atoms, even preventing the observation of any wurtzite peaks for Co concentrations higher than 17%. On the other hand, the absence of peaks corresponding to cubic CoO indicates that no detectable amounts of mixed crystalline $(\text{ZnO})_x(\text{CoO})_{1-x}$ phases are present, and hence, Co atoms should be fully incorporated into the ZnO lattice.²¹ Even though the XRD cannot exclude the presence of additional nanoscopic or amorphous phases, the magnetic measurements discussed below illustrate the former hypothesis.

Figure 3(a) shows a set of optical transmission spectra corresponding to blue-colored $\text{Zn}_{1-x}\text{Co}_x\text{O}$ thin films at 0.06 and 0.17 compared with the ZnO reference sample. In the visible region, high transmittance is exhibited by all films, which is a usual feature of ternary oxides grown by electrodeposition using DMSO as solvent.¹⁷ The interference fringes, which are the consequence of the exceptional smoothness of these films, are evident. The fundamental absorption edge, which is very sharp for the ZnO sample, becomes deformed and shifts to the red as the Co content increases. Such a deformation can be decomposed into two parts: (a) a strong band arising probably from the hybridization of excited $3d$ Co levels with the conduction band, which is responsible for the shift of the absorption edge to higher wavelengths, and (b) an increase in the band-to-band fundamental transition responsible for the transmission “step” appearing at wavelengths lower than the ZnO band gap. This effect is coherent with the substitution of Zn by a lighter element (Co).²² The increase in Co content is also accompanied by a wide absorption band centered at about 600 nm. This absorption band is composed of the superposition of

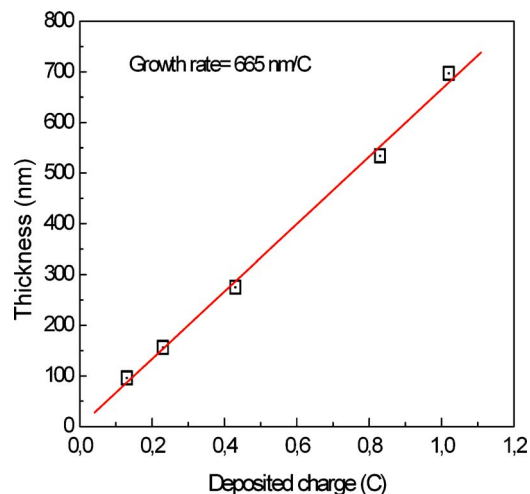


FIG. 4. (Color online) Thickness of several $\text{Zn}_{0.83}\text{Co}_{0.17}\text{O}$ films as a function of the deposited electrical charge.

three other bands labeled as arrows. The presence of interference fringes disturbs the position of the centers of the absorption bands. However, when the interference fringes do not appear, the three bands are located at 567, 610, and 654 nm, which are very near to the reported values.^{2,3,9} These bands are characteristic of $d-d$ transitions in tetrahedrally coordinated Co^{2+} , which are substituting Zn^{2+} cations.²³ This interpretation supports the former deductions of the structural characterization as well. The observed blue color of the samples is due to these three absorption bands located in the green-red region. Higher Co concentrations imply a more intense blue color in the films.

In order to measure the growth rate of the films, several samples having different deposited electrical charges were prepared from the same bath. The thicknesses of the films were obtained from the interferential fringes of the transmission spectra. Figure 4 shows the thicknesses of the growing thin films as a function of the deposited electrical charge after subtracting the calculated thickness for the FTO layer. A good linearity between the thickness of the films and the deposited electrical charge is observed. A growth rate of 665 nm/C is calculated from the slope of the linear fit, which is slightly lower than that obtained for ternary ZnCdO.¹⁷ Taking into account the density and unit cell volume for ZnO, a theoretical value of 750 nm/C for the m/Q ratio, which is close to the measured value, is calculated.

The magnetic properties of compound $\text{Zn}_{0.83}\text{Co}_{0.17}\text{O}$ under the form of χT vs T (χ being the magnetic susceptibility) is shown in Fig. 5. These values were scaled from the magnetization plot (Fig. 6) where the saturation magnetization was fixed to 3 Bohr magnetons (expected value for a $S = 3/2$ with $g = 2$). This scaling was applied to the magnetic susceptibility data.

The χT values remain nearly constant at a wide range of temperatures and smoothly decrease at low temperatures. In principle, the slight decrease in χT at low temperatures could be attributed to intermolecular interactions and/or zero-field splitting (zfs) effects. For a d^7 ion in a tetrahedral environment (T_d symmetry group), the ground and the first excited state are 4A_2 and 4T_2 , respectively, arising from the 4F free

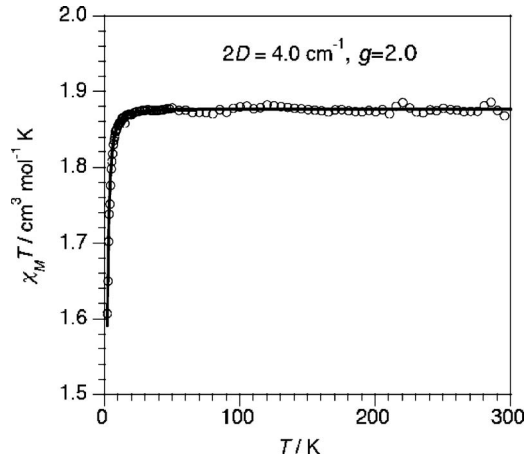


FIG. 5. Thermal dependence of the χT product for $\text{Zn}_{0.83}\text{Co}_{0.17}\text{O}$ sample. The solid line is the best-fit curve through Eq. (2a)–(2c).

ion ground state. The presence of a ligand field component of symmetry lower than cubic can cause the magnetic moment to vary with T as the spin degeneracy of the 4A_2 ground state is then lifted. Under a tetragonal distortion (D_2 symmetry group), this state is split into an orbital singlet 4B_2 and an orbital doublet 4E at energies Δ_z and Δ_{xy} , respectively (see Fig. 7). The quartet spin ground state 4A_2 is removed by the combined action of the spin-orbit interaction and the tetragonal crystal field leading to two Kramers doublets (zfs).^{24,25}

Formally, this behavior can be treated as an $S=3/2$ spin state under the action of the spin Hamiltonian of Eq. (1) where $2D$ represents the splitting into two Kramers doublets in the absence of a magnetic field. In the present notation, positive D values stabilize the $\pm 1/2$ state. The expression of the magnetic susceptibility in Eq. (2a)–(2c) is easily derived from Hamiltonian (1) (the parameters therein involved have their usual meaning)

$$\hat{H} = D[\hat{S}_z^2 - (1/3)S(S+1)] + g^{\parallel}\beta\hat{H}\hat{S}_z + g^{\perp}\beta\hat{H}[\hat{S}_x + \hat{S}_y], \quad (1)$$

$$\chi_{\parallel} = \frac{N\beta^2 g_{\parallel}^2}{4kT} \left\{ \frac{1 + 9 \exp(-2D/kT)}{1 + \exp(-2D/kT)} \right\}, \quad (2a)$$

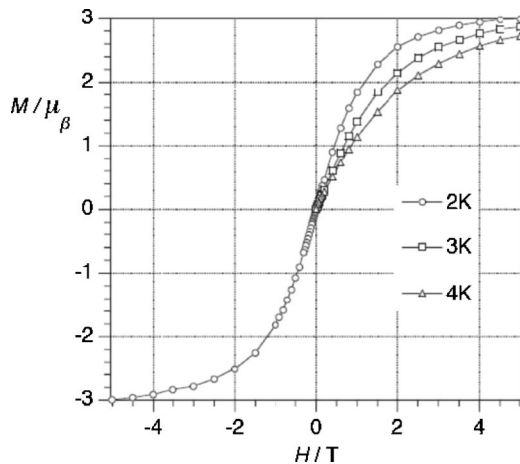


FIG. 6. Isotherms ($2 \leq T \leq 4$) of the magnetization vs H plot for a $\text{Zn}_{0.83}\text{Co}_{0.17}\text{O}$ film.

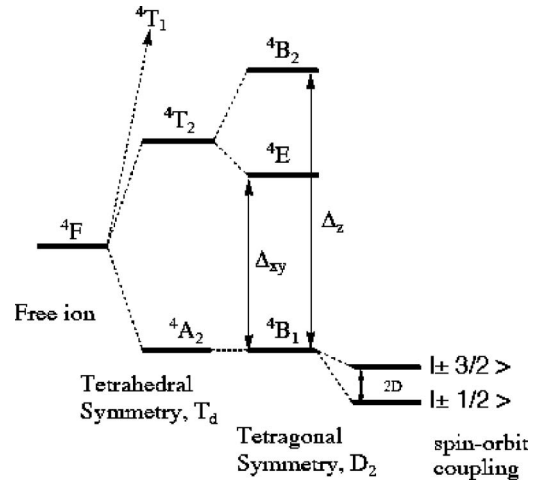


FIG. 7. Scheme of the splitting of energy levels of the 4F free ion ground state under the influence of crystal symmetries.

$$\chi_{\perp} = \frac{N\beta^2 g_{\perp}^2}{kT} \left\{ \frac{1 + (3kT/4D)[1 - \exp(-2D/kT)]}{1 + \exp(-2D/kT)} \right\}, \quad (2b)$$

$$\chi_{\text{av}} = \frac{\chi_{\parallel} + 2\chi_{\perp}}{3}. \quad (2c)$$

Least squares fitting of the experimental data through this expression leads to $D=2.0(2) \text{ cm}^{-1}$. The good fit achieved indicates that, most likely, the zfs is the responsible factor for the slight decrease in χT and that no significant magnetic interactions between Co(II) centers are present. This fact suggests that the Co(II) ions must be well isolated from each other into the film. The magnetization plot (Fig. 6) also supports the occurrence of a magnetically isolated paramagnetic species. Moreover, measurements of χT performed on films with minor Co content exhibit analogous magnetic behavior.

The paramagnetic behavior displayed by the electrodeposited $\text{Zn}_{1-x}\text{Co}_x\text{O}$ films rejects the existence of isolated CoO , which exhibits an antiferromagnetic behavior,²⁶ and confirms that Co^{2+} ions are fully incorporated into the ZnO lattice.

IV. CONCLUSION

In conclusion, ternary $\text{Zn}_{1-x}\text{Co}_x\text{O}$ alloy films have been prepared by means of cathodic electrodeposition at low temperature and atmospheric pressure. The concentration of Co is fixed by varying the molar ratio between the CoCl_2 and ZnCl_2 precursors in the starting bath. The electrodeposited $\text{Zn}_{1-x}\text{Co}_x\text{O}$ films exhibit a wurtzite structure with a preferred orientation in the (002) direction, and no peaks referred to cubic CoO are observed. In the visible spectral range, $\text{Zn}_{1-x}\text{Co}_x\text{O}$ thin films have good transmittance, and the observation of a redshift on the absorption edge as well as the existence of three absorption bands confirms the incorporation of Co in the ZnO lattice. The thickness of the ternary films can be precisely controlled through the amount of deposited electrical charge. The behavior of the product χT vs T suggests the paramagnetic nature of the ternary $\text{Zn}_{1-x}\text{Co}_x\text{O}$

films. This fact is due to a homogeneous distribution of Co(II) ions, which are isolated from each other.

ACKNOWLEDGMENTS

This work was supported by the Spanish Government MEC through Grant No. MAT2006–02279. Thanks are given to the staff of *Servei de Microscopia (UPV)* for their assistance during SEM and EDX measurements.

- ¹T. Dietl, H. Ohno, and F. Matsukura, *Phys. Rev. B* **63**, 195205 (2001).
- ²A. Dinia, J. P. Ayoub, G. Schmerber, E. Beaurepaire, D. Muller, and J. J. Grob, *Phys. Lett. A* **333**, 152 (2004).
- ³G. L. Liu, Q. Cao, J. X. Deng, P. F. Xing, Y. F. Tian, Y. X. Chen, S. S. Yan, and L. M. Mei, *Appl. Phys. Lett.* **90**, 052504 (2007).
- ⁴T. Shi, S. Zhu, Z. Sun, S. Wei, and W. Liu, *Appl. Phys. Lett.* **90**, 102108 (2007).
- ⁵Y. Belghazi, G. Schmerber, S. Colis, J. L. Rehspringer, A. Dinia, and A. Berrada, *Appl. Phys. Lett.* **89**, 122504 (2006).
- ⁶J. H. Kim, H. Kim, D. Kim, Y. E. Ihm, and W. K. Choo, *Physica B (Amsterdam)* **327**, 304 (2002).
- ⁷J. H. Kim, H. Kim, D. Kim, Y. E. Ihm, and W. K. Choo, *J. Eur. Ceram. Soc.* **24**, 1847 (2004).
- ⁸S. W. Lim, D. K. Hwang, and J. M. Myoung, *Solid State Commun.* **125**, 231 (2003).
- ⁹S. Ramachandran, A. Tiwari, and J. Narayan, *Appl. Phys. Lett.* **84**, 25 (2004).
- ¹⁰H. Ndilimabaka, S. Colis, G. Schmerber, D. Muller, J. J. Grob, L. Gravier, C. Jan, E. Beaurepaire, and A. Dinia, *Chem. Phys. Lett.* **421**, 184 (2006).
- ¹¹W. Prellier, A. Fouchet, Ch. Simon, and B. Mercey, *Mater. Sci. Eng., B* **109**, 192 (2004).
- ¹²K. Samanta, P. Bhattacharya, R. S. Katiyar, W. Iwamoto, P. G. Pagliuso, and C. Rettori, *Phys. Rev. B* **73**, 245213 (2006).
- ¹³Th. Pauporté, A. Goux, A. Kahn-Harari, N. De Tacconi, C. R. Chenthamarakshan, K. Rajeshwar, and D. Lincot, *J. Phys. Chem. Solids* **64**, 1737 (2003).
- ¹⁴J. Cembrero, A. Elmanouni, B. Hartiti, M. Mollar, and B. Marí, *Thin Solid Films* **451–452**, 198 (2004).
- ¹⁵B. Marí, F. J. Manjón, M. Mollar, J. Cembrero, and R. Gómez, *Appl. Surf. Sci.* **252**, 2826 (2005).
- ¹⁶H. Ishizaki and N. Yamada, *Electrochem. Solid-State Lett.* **9**, C178 (2006).
- ¹⁷M. Tortosa, M. Mollar, and B. Marí, *J. Cryst. Growth* **304**, 97 (2007).
- ¹⁸D. Gal, G. Hodes, D. Lincot, and H. W. Schock, *Thin Solid Films* **361–362**, 79 (2000).
- ¹⁹R. Jayakrishnan and G. Hodes, *Thin Solid Films* **440**, 19 (2003).
- ²⁰T. Y. Yoshida, D. Komatsu, N. Shimokawa, and H. Minoura, *Thin Solid Films* **451–452**, 166 (2004).
- ²¹D. W. Ma, Z. Z. Ye, J. Y. Huag, L. P. Zhu, B. H. Zhao, and J. H. He, *Mater. Sci. Eng., B* **111**, 9 (2004).
- ²²J. A. Sans, J. F. Sánchez-Royo, J. Pellicer-Porres, A. Segura, E. Guillotel, G. Martínez-Criado, J. Susini, A. Muñoz-Páez, and V. López-Flores, *Superlattices Microstruct.* **42**, 226 (2007).
- ²³P. Koidel, *Phys. Rev. B* **15**, 2493 (1977).
- ²⁴O. Kahn, *Molecular Magnetism* (VCH, New York, 1993).
- ²⁵N. Durán, W. Clegg, L. Cucurrull-Sánchez, R. A. Coxal, H. R. Jiménez, J. M. Moratal, F. Lloret, and P. González-Durate, *Inorg. Chem.* **39**, 4821 (2000).
- ²⁶C. M. Sorenson, *Nanoscale Materials in Chemistry*, edited by K. J. Klaibunde (Wiley, New York, 2001), Chap. 6, p. 191.